Plasma Sci. Technol. **25** (2023) 025405 (15pp) https://doi.org/10.1088/2058-6272/ac8fca

Comparison of pulse-modulated and continuous operation modes of a radio-frequency inductive ion source

Ilya ZADIRIEV*, Elena KRALKINA, Konstantin VAVILIN, Alexander NIKONOV and Georgy SHVIDKIY

Physical Electronics Department, Faculty of Physics, Lomonosov Moscow State University, Moscow 119991, Russia

E-mail: iizadiriev@yandex.ru

Received 28 May 2022, revised 29 August 2022
Accepted for publication 6 September 2022
Published 6 January 2023

Abstract

The paper describes an experimental study of the characteristics of a pulse-modulated radio-frequency (RF) discharge sustained at low pressures, typical of the operating modes of RF gridded ion sources. The motivation for the study is the question of whether the RF pulse-modulated mode can increase the efficiency of the ion source. The ion current values extracted from an RF inductive ion source operating in continuous and pulse-modulated modes were compared. The experimental data were also compared with the parameter calculations based on a 0D numerical model of the discharge. The measurements showed that the pulse-modulated operation mode of the RF ion source had a noticeable advantage when the power of the RF generator was 140 W or lower. However, as the generator power increased, the advantage was lost because the pulse-modulated operation mode, having a higher RF power instant value, entered the region of existence sooner than the continuous mode, where the ion production cost begins to grow with RF power.

Keywords: discharge, plasma, radio frequency (RF), pulse, electrons, ions

(Some figures may appear in colour only in the online journal)

1. Introduction

The pulse-modulated mode is one of the most popular and interesting modes of gas discharge from both the physical and practical points of view. A comparison of the AC discharge parameters in continuous and pulse-modulated modes [1–3] identified a number of advantages of the latter. Indeed, in the pulse-modulated mode, while maintaining the average power supplied to the discharge, it is possible to deposit higher values of radio-frequency (RF) power into the plasma during the active period of the pulse. In a number of cases, this leads to the achievement of higher mean values of plasma density over the period.

It is not surprising that the wide practical use of RF discharges, in particular, in the problems of etching semiconductor wafers, has led to the appearance of numerous works [4–17] studying the pulse-modulated operation mode of plasma reactors.

In [4] the pulse-modulated discharges in argon and argon-chlorine mixture were studied at 13.56 MHz, duty cycles between 10% and 70%, and pulse repetition frequencies between 3 and 20 kHz. It was shown that after the ignition of a pulse-modulated inductive discharge in argon and its mixture with chlorine, during the first 5–30 RF voltage pulses, the discharge was sustained in the capacitive mode. The plasma potential in the active part of the pulse reaches hundreds of volts, and the electron density has relatively low values typical for a capacitive RF discharge. Later, the discharge jumps into the H-mode, the plasma potential reduces and electron density grows. The authors of [5] observed a transition from the E-mode to the H-mode during every active part of the pulse. The transition was carried out not abruptly,

* Author to whom any correspondence should be addressed.

but smoothly, so it was not possible to quantify the contribution of the capacitive and inductive components to maintain the discharge. It should be noted that the rise time of the equilibrium values of the electron concentration observed in [5] is quite long. This may be a consequence of the implementation of the E-mode of the discharge at the initial moments of time of the active part of the pulse.

In [6, 7], the time dependencies of the electron temperature and ion flux in the volume of the plasma source were studied. It was shown that at the beginning of the pulse's active part, the ion flux reached its maximum near the walls of the plasma source, where the antenna was located. Then, as the equilibrium values of the plasma density were approached, the spatial distribution of the ion current became 'convex', i.e. it reached a maximum near the source axis. The effect weakened as the pressure decreased and as one approached the substrate. The authors of [6, 7] explained the observed effects by the nonlocal kinetics of charged particles under the experimental conditions and by the patterns of diffusion.

The electron temperature [6] rapidly increases at the initial moment of the pulse, then decreases, and finally reaches equilibrium values. The maximum temperature values depend on the electron density that is realized in the discharge in the afterglow stage before the onset of the active phase of the pulse. An increase in the electron temperature at the initial moment of the pulse was also observed in experiments [5, 8] and was also confirmed by numerical calculations performed using the global discharge model [9].

References [9–13] present numerical models of a pulse-modulated inductive RF discharge. The main practical focus of the works is related to the search for ways to improve the etching processes in plasma reactors. The time dependencies of the plasma parameters and the time evolutions of their spatial distributions are calculated. The conditions are found to increase the plasma homogeneity near the substrate.

The authors of [14, 15] studied the pulse-modulated inductively coupled discharge in Ar and Ar/CF_4 mixture. They measured the time dependencies of input power, electron density, effective electron temperature, relative light intensity, and electron energy probability function. Two peaks of the input power were registered: one being determined by the RF power source, while the second one by the plasma properties and the state of the matching box. The overshoot behavior of the electron density and light intensity in the initial pulse stage was revealed. The overshooting phenomena decrease with the decrease of the RF power and the increase of the gas pressure.

The authors of [16] performed fully 3D, time dependent measurements of the RF magnetic field, electron density, and electron temperature for an inductively coupled discharge sustained in argon. The measurements showed that during a single RF cycle, the 3D current first reached maximum just below the planar coil and then moved toward the center of the plasma reactor. A computer simulation of the experiment reproduced the phase dependent behavior.

The use of the halogen gas additives in the argon inductively coupled discharge is accompanied by the instabilities, E–H transitions and ignition delays when applying power on the next pulse. Based on computer simulation, it is proposed in [17] to improve the situation by maintaining a low-level power environment during 'pulse-off' to keep the minimum plasma density.

References [4–17] primarily focus on ways to improve the operating modes of technological plasma reactors. Another type of plasma device widely used in terrestrial and space technologies is ion sources based on an inductive RF low-pressure discharge ($p < 1$ mTorr). Significant interest in RF inductive ion sources (RF IISs) is due to the long life span and the possibility of obtaining dense plasma at relatively low power values. This makes RF IISs interesting for use in space as ion thrusters [18–22]. Previously, the analysis of the possibilities to use the pulse-modulated mode of RF IISs was not considered in the literatures. This paper presents the first results of studying such possibilities. The motivations for starting the research were as follows. First, during the active part τ_{on} of the pulse of duration τ, the power of the RF generator can significantly exceed the average over the period. This should facilitate the ignition of the discharge, reduce the influence of the parasitic capacitive component, and also increase the plasma concentration averaged over τ due to the fact that electron temperature in the initial part of the pulse is higher than that in the continuous mode. In addition, the electron density can rise when stepwise ionisation is significant. Second, during the passive part of the pulse with duration τ_{off}, when the power of the RF generator is zero, the electron concentration, as well as the ion current extracted from the source, does not immediately drop to zero. This may improve the performance of the RF IIS. It should be noted that the gain in the average ion current obtained during the pulse compared to the continuous mode can be achieved only if the plasma density rise time at its leading edge is shorter than the plasma deionisation time. In this regard, this work pays the main attention to studying the influence of the physical features of an inductive RF discharge on the time necessary to reach the equilibrium plasma characteristics. The influence of the features of the matching system on the establishment of equilibrium was not considered. The measurements were carried out at an RF generator frequency of 13.56 MHz and pulse repetition rates of 5, 10, and 20 kHz (pulse durations τ are 200, 100, and 50 μs). The duty cycles (τ_{on}/τ) were 17%, 25%, 50%, and 75%. In addition to the experimental data, the paper presents the results of numerical simulation of the time dependencies of the main plasma parameters using a 0D global discharge model. The experimental results are compared with the calculated ones.

2. Experimental setup and measurement technique

A diagram of the laboratory prototype of an RF IIS is shown in figure 1. The RF IIS consists of a gas discharge chamber (GDC), a gas distributor, an RF power input unit, and an ion-optical system (IOS). The GDC made from quartz is 10 cm in diameter and 5 cm in length. The RF power input unit is a helical antenna located on the side surface of the GDC. The 3.5-turn water-cooled antenna is made of a copper tube with a diameter of 3 mm.

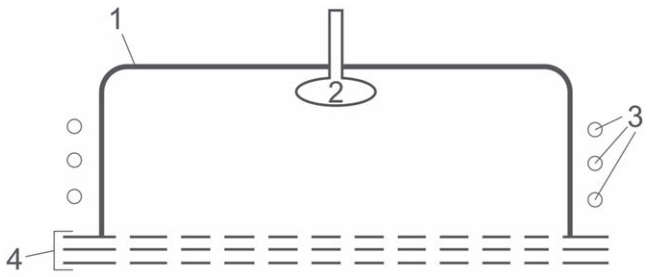

Figure 1. Scheme of the RF IIS. 1—GDC made of dielectric material, 2—gas distributor, 3—helical antenna, 4—three-grid IOS.

In order to investigate the influence of the capacitive component on the pulse-modulated discharge parameters, the natural parasitic coupling of the antenna and plasma was enhanced. For this, a hybrid discharge was organised [23, 24]; namely, in addition to the antenna, an electrode was located on the end surface, which was connected in parallel to the antenna through a separating capacitance of 20 pF. The connection diagram is shown in figure 2. In this scheme, two channels of RF power input, i.e. the capacitive and the inductive ones, coexist in the plasma volume. At low powers of the RF generator, the power is coupled to the discharge mainly through the capacitive channel, and at high powers—through the inductive one. The larger the area of the additional electrode and the value of the separating capacitance, the greater the contribution of the capacitive channel [23, 24].

The IOS consists of three perforated titanium electrodes. The transparency of the IOS is 60%. The distance between the electrodes is 0.7 mm. Voltage was applied to the IOS electrodes according to the acceleration-deceleration scheme.

To organize an inductive RF discharge, the ends of the antenna were connected to a Cesar 1310 RF generator through a matching system. The generator frequency is 13.56 MHz; the power range is 0–1000 W. In the entire studied range of experimental conditions, it was possible to obtain the value of the reflected RF power less than 10% of the incident power. The experiments were carried out at RF generator powers of 50–600 W, at pulse repetition rates of 5, 10, and 20 kHz, and operating cycles of 17%, 25%, 50%, and 75%. The indication of the RF generator power corresponds to the power output by the generator within the operating cycle of the pulse, while the average power of the RF generator output by the generator within the pulse is determined by the formula:

$$P_{\text{on}} = P_{\text{gen}} \frac{\tau}{\tau_{\text{on}}} \tag{1}$$

Figure 3 shows the time dependence of the signal from the Rogowski coil used to measure the current flowing through the antenna. The duration of the leading edge of the pulse was 9 μs, and that of the trailing edge was 5 μs. Typical fractions of RF power input to the discharge plasma with the RF IIS operating in continuous mode were in the range of 50%–65% and were determined using technique from [25].

The plasma potential in the GDC of the operating plasma source is equal to the potential of the emission electrode up to a floating potential. In this work, the potential of the emission electrode was 1000 V. Under such conditions, it is difficult to carry out probe measurements to find the concentration and temperature of electrons. In this regard, we studied the time-dependence of the intensity of the spectral lines, since the intensity values depend both on the concentration and on the electron energy distribution function.

The plasma radiation from the central orifice of IOS was directed by a system of lenses to the entrance slit of an MDR-41 monochromator. At the output of the monochromator, there was a photomultiplier FEU-100, the signal of which after amplification and conversion was stored in a computer. The spectrum was scanned in the range of 400–600 nm. The measurements showed that both atomic and ionic lines were presented in the plasma emission spectrum. Subsequently, the main attention was focused on the time dependencies of the ArI 420.1 nm and ArII 480.6 nm lines.

The measurements were carried out at argon flow rates of 10 and 16 sccm. These flow rates give estimated concentrations of argon inside the GDC at 1.8×10^{14} cm^{-3} and 2.8×10^{14} cm^{-3}, respectively (not taking into account argon losses due to ion current through IOS). Pressure in the vacuum chamber during the RF IIS operation was 0.3–0.4 mTorr.

3. Experimental results

The goal of the present experiments was to study the influence of the pulse-modulated discharge external parameters (the power of the RF generator, argon flow rate, the pulse duration τ, and the duty cycle τ_{on}/τ) on the time dependencies of the internal discharge parameters, and also to compare the ion current values obtained in pulse-modulated and continuous modes of the RF IIS operation.

Let us first consider the data obtained during the continuous operation of the ion source. Note that the two most important characteristics of an ion source are the 'ion cost', i.e. the $P_{\text{gen}}/I_{\text{b}}$ and gas efficiency, i.e. $I_{\text{b}}/(ef_{\text{v}})$, where I_{b}, e and f_{v} are the ion beam, electron charge and gas flow rate. Typical dependencies of the RF generator power P_{gen} required to extract the ion beam current of a given value I_{b} on the argon flow rate f_{v} are shown in figure 4. At high gas flow rates, the values of P_{gen} are relatively small. However, they begin to grow rapidly as f_{v} decreases. The greater the value of the extracted ion current, the greater the growth rates of P_{gen}, and the earlier the ascending region of the required values of P_{gen} starts.

The numerical calculations performed in [26] showed that, in the region of high gas flow rates, an increase in the ion current with an increase in P_{gen} occurred due to an increase in the electron concentration at an almost constant electron temperature. On the contrary, in the region of small f_{v}, when the atomic density in the plasma volume is low, a certain value of I_{b} is maintained due to a significant increase in the electron temperature T_{e}, enhancing the ionisation rate. The larger the value of I_{b}, the larger values of T_{e} and P_{gen} are necessary. Thus [26], the operating modes of the RF IIS can be divided into two parts: the region of large f_{v}, where the ion

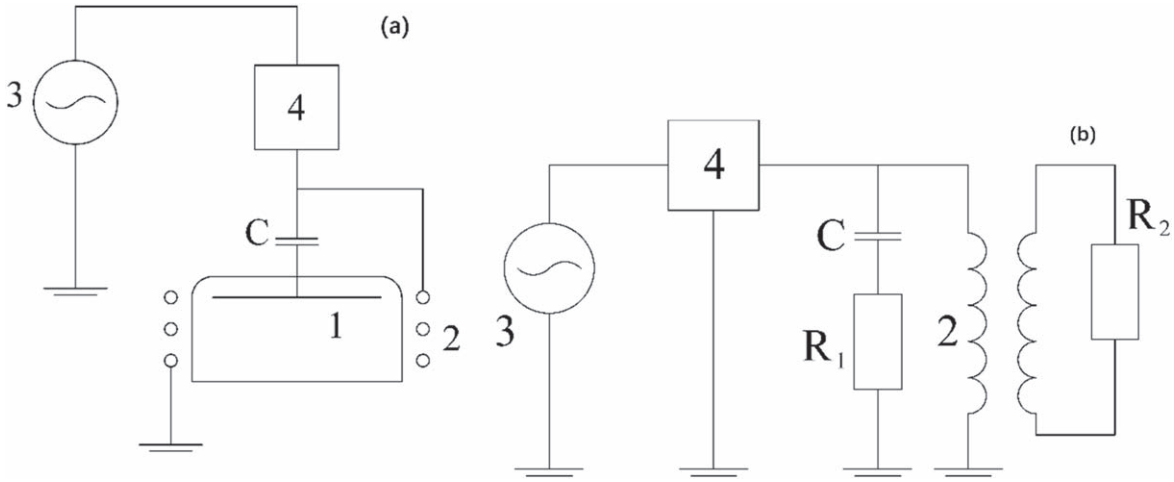

Figure 2. Hybrid discharge setup (a) and its electric circuit (b). 1—capacitive electrode, 2—helical antenna, 3—RF power source, 4—matching circuit, C—separating capacitance, R_1—plasma impedance in the capacitive channel, R_2—plasma impedance in the inductive channel.

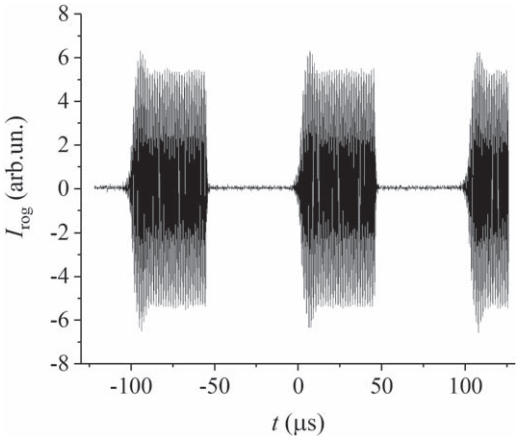

Figure 3. Time dependence of the Rogowski coil signal I_{rog}.

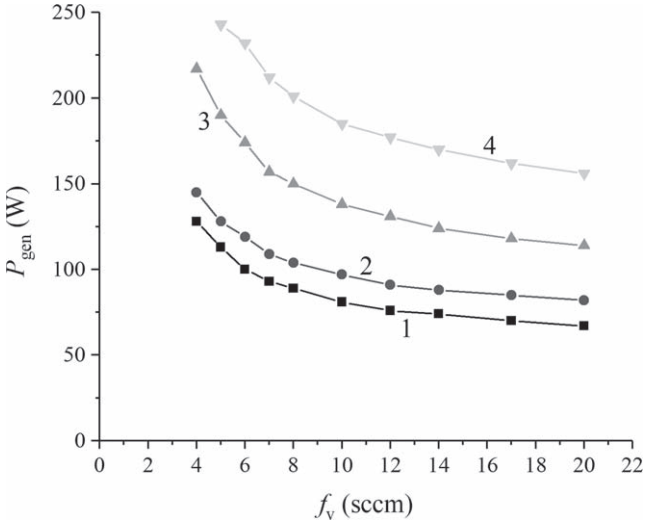

Figure 4. Dependence of the power of the RF generator P_{gen}, required to extract the ion current of a given value, on the argon flow rate f_v. Extracted current I_{beam}: 80 mA (1), 100 mA (2), 150 mA (3), 200 mA (4).

current grows at a fixed electron temperature, and the region of small f_v, where a significant increase in T_e is required for the growth of the ion current.

Taking into account the above considerations, the research team studied the pulse-modulated mode of the RF IIS operation at two argon flow rates belonging to two different ranges. First, let us consider the range of high argon consumption. Here, instead of measuring $I_b(t)$, the researchers studied the time dependencies of plasma radiation intensity. The reason was a number of breakdowns between the IOS electrodes arising due to the shortcomings of the pumping system. Figures 5 and 6 show the change in the intensity of the atomic and ionic lines ArI 420.0 nm and ArII 480.6 nm with time at different values of the RF generator power.

As can be seen, at an RF generator power of 100 W, the intensity of atomic lines reaches an equilibrium value in a time of about 20 μs. For large values of P_{gen}, this value is reduced to 10 μs. The decrease in the plasma radiation intensity after turning off the RF generator power occurs over times of the order of 15 μs. These conclusions are valid for all considered pulse repetition rates (see figure 7). The achievement of equilibrium values by ionic lines lags behind atomic ones. This is clearly seen in figure 8.

Figure 9 shows the change in the time dependencies of the intensities of atomic and ionic spectral lines with a variation in the duration of the working cycle τ_{on} while maintaining the pulse duration τ and average RF power $P_{av} = P_{gen}\tau_{on}/\tau$. A change in τ_{on} is accompanied by an increase in the RF power coupled to plasma in the active part of the pulse; therefore, a decrease in the duty cycle leads to an increase in the luminescence intensity. The relative increase in the ionic line intensity significantly outstrips the increase in the intensity of the atomic line with τ_{on}/τ changing from 50% to 17%. As τ_{on}/τ decreases to 17%, the intensity of the plasma radiation does not reach the equilibrium values. This is especially noticeable when considering the behaviour of the ionic line intensity. The latter is related to the delay in the

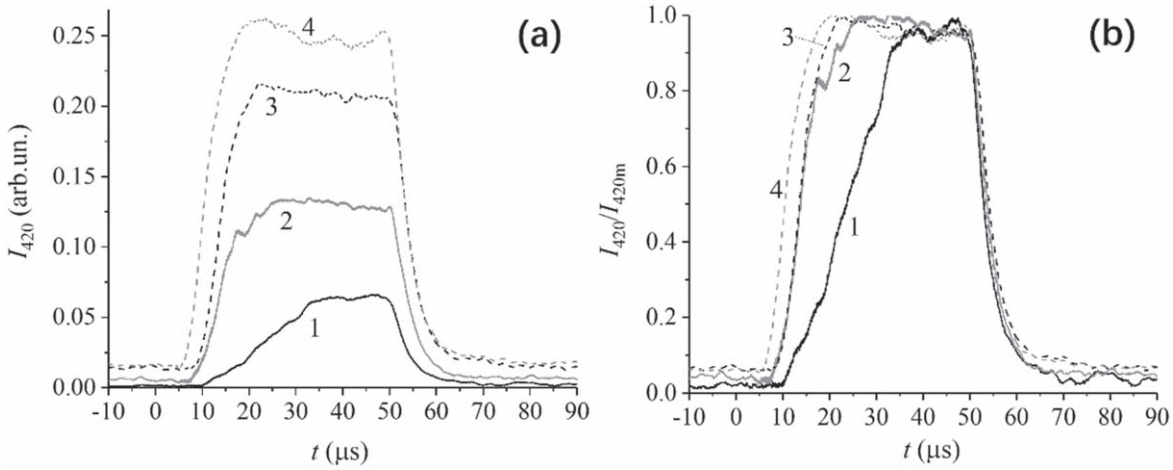

Figure 5. Time dependence of the intensity of the 420.0 nm argon atomic line (a) and the same curves normalised to the maximum value (b). Numbers denote different P_{gen}: 100 W (1), 200 W (2), 300 W (3), 400 W (4). The pulse duration is 100 μs, the duty cycle is 50%, argon consumption is 16 sccm.

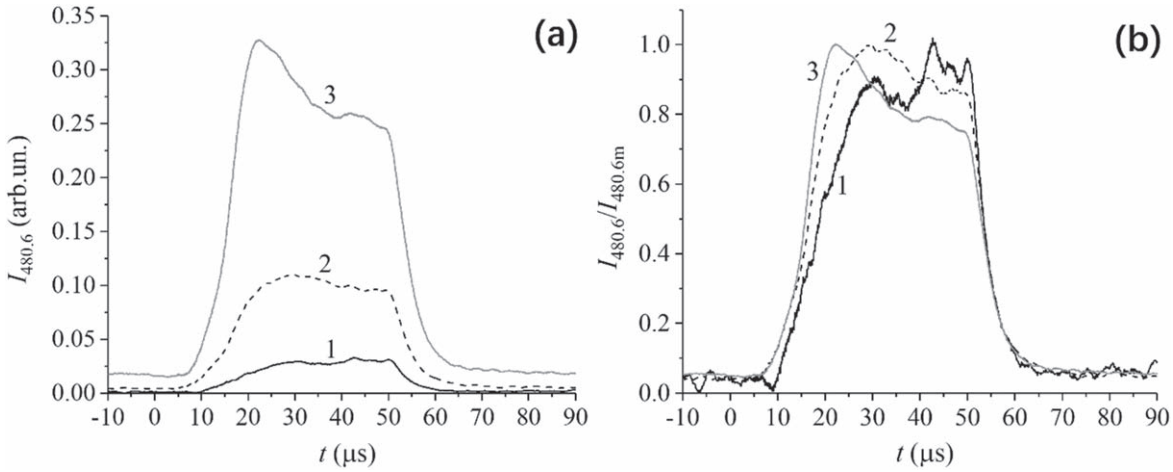

Figure 6. Time dependence of the intensity of the 480.6 nm argon ion line (a) and the same curves normalized to the maximum value (b). Numbers denote different P_{gen}: 200 W (1), 300 W (2), 400 W (1). The line was not detected with P_{gen} of 100 W. The pulse duration is 100 μs, the duty cycle is 50%, argon consumption is 16 sccm.

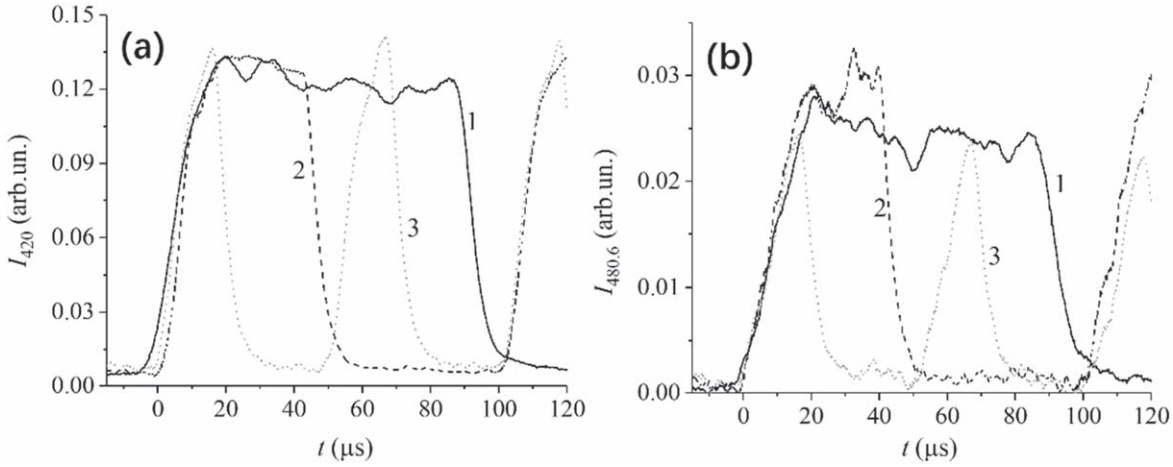

Figure 7. Time dependence of the intensity of the argon atomic (a) and ionic (b) spectral lines for the cases: $\tau = 200$ μs (1), $\tau = 100$ μs (2), $\tau = 50$ μs (3). The duty cycle is 50%, argon consumption is 16 sccm.

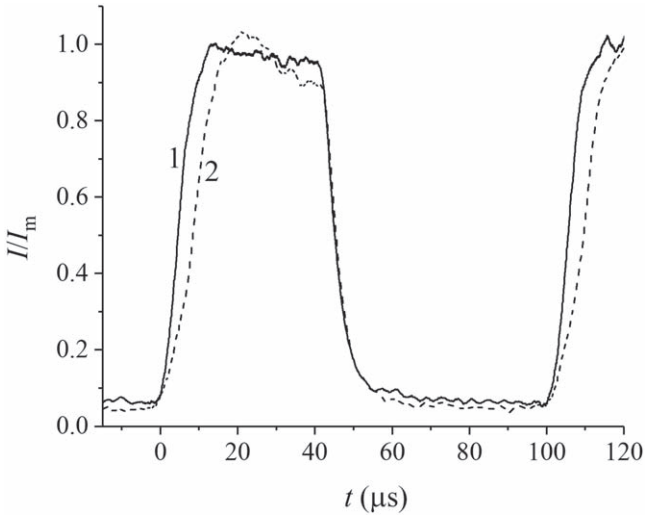

Figure 8. Time dependence of the normalised values of the intensity of the argon atomic and ionic spectral lines. Atomic line (1), ionic line (2). The power of the RF generator is 300 W, the pulse duration is 100 μs, the duty cycle is 50%, argon consumption is 16 sccm.

establishment of the equilibrium values of ionic lines in comparison with atomic ones.

The dependencies of the maximum values of the atomic and ionic lines radiation intensity, achieved within the period of the pulse, on the power of the RF generator at various τ and τ_{on}/τ are shown in figure 10. Provided that $\tau_{on}/\tau \geqslant 25\%$, the intensity of ArI 420.0 nm increases linearly with the power of the RF generator, while the intensity of the ArII 480.6 ionic line increases quadratically.

The linear nature of the dependence of the atomic lines on the RF generator power indicates the predominance of the direct excitation of argon energy levels under the considered experimental conditions. The quadratic dependence of the ionic line is due to the fact that under the conditions of the ion source operation, where the degree of ionisation is high, the excitation of the ionic spectral lines is possible as a result of two processes: ionization with the excitation of the argon atoms and the excitation of the ions in collisions with electrons. The second process is quadratic with respect to the electron concentration, which, in turn, is proportional to the RF generator power under the supposition that electron temperature is constant.

In the range of low flow rates (7–12 sccm), the time dependencies of the ion current were studied. Here the assumption that the electron temperature is constant with increasing I_b and P_{gen} is inapplicable.

It is well known that any inductive RF discharge has an irremovable 'parasitic' capacitive channel due to capacitances between coils of RF antenna as well as capacitances between RF antenna and metallic parts in contact with plasma. The presence of the capacitive component affects the transition between the E-mode and the H-mode and can influence the process of reaching a steady state. Because of that, the influence of the inductive discharge capacitive component on the time of the establishment of equilibrium I_b values was studied. For this purpose, a hybrid RF discharge scheme was used (see figure 2). The results obtained are shown in figure 11. They clearly prove that the presence of the capacitive component is accompanied by a significant delay in the equilibrium establishment. The time required to achieve equilibrium in a hybrid discharge is close to the values obtained in [5]. Recall that the authors of [5] observed a transition from the E-mode to the H-mode during each pulse.

Typical time dependencies $I_b(t)$ measured in experiments with an inductive discharge at various RF generator powers and different τ_{on}/τ are shown in figure 12. As can be seen, the times of the leading and trailing fronts of the ion current are close to the values typical of the time dependencies of plasma radiation intensities. However, the dependencies of the maximum (equilibrium) values of the ion current on the RF generator power and the duty cycle differ from linear (see figure 13). The growth of P_{gen} is accompanied by a slowdown in the growth of I_b.

The dependencies of the ion current on the RF generator power, obtained in pulse-modulated and continuous modes of the RF IIS operation, are shown in figure 14. It can be seen that the pulse-modulated mode has a noticeable advantage at low powers of the RF generator. However, as P_{gen} increases, the advantage is lost. In order to understand the physical reasons for the obtained experimental results, numerical calculations were performed.

4. Numerical model of a pulse-modulated inductive RF discharge

The numerical global model of a pulsed inductive RF discharge, which makes it possible to calculate the time dependence of the density of the main plasma components, is based on the following assumptions:

- The plasma consists of neutral argon atoms in the ground, metastable and resonant states, as well as ions and electrons.
- The electron energy distribution function is Maxwellian.
- The plasma quasi-neutrality has been achieved.
- The discharge is immediately ignited in the inductive H-mode.

It is assumed that ions appear in a discharge as a result of collisions of electrons with the atoms in the ground state (Ar_0), metastable (Ar_1), and resonance (Ar_2) states, as well as a result of Penning ionisation; ions are lost in the discharge volume as a result of three-particle electron–ion recombination, as well as on the walls of the plasma source. The metastable atoms are populated due to the direct excitation of ground state atoms by electrons, electron collisions of the second kind with atoms in a resonant state, and also due to three-particle recombination. Atoms in the metastable state are depopulated as a result of ionization by electrons, collisions of the second kind with electrons with the formation of the ground state atoms, due to Penning ionisation, and due to escape to the walls of the plasma source. Atoms in the resonant state are populated as a result of direct excitation of atoms and stepwise excitation from the

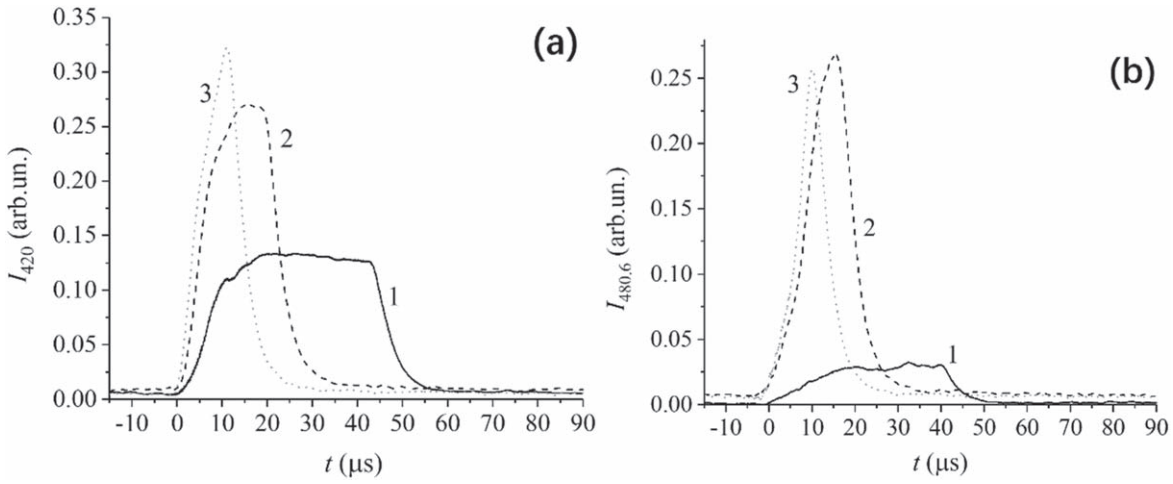

Figure 9. Time dependence of the intensity of the argon atomic (a) and ionic (b) spectral lines for the cases: $\tau_{on}/\tau = 50\%$ (1), $\tau_{on}/\tau = 25\%$ (2), $\tau_{on}/\tau = 17\%$ (3). The pulse duration is 100 μs, argon consumption is 16 sccm, RF generator power averaged over the pulse period is 100 W.

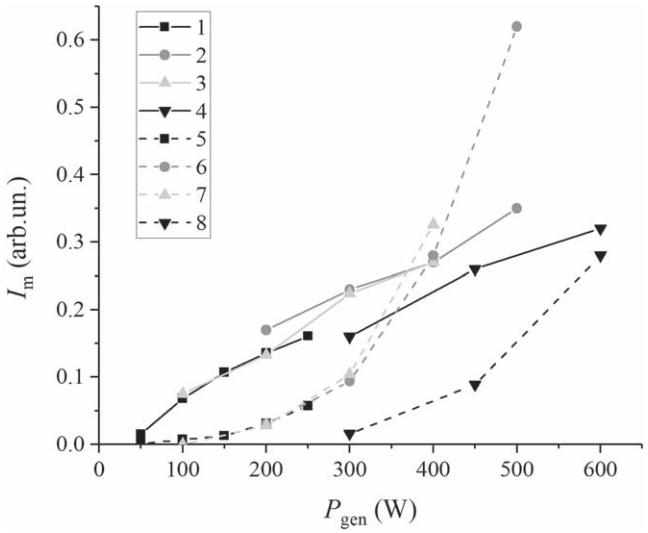

Figure 10. Dependencies of the maximum values I_m of the radiation intensities of atomic I_{420} and ionic $I_{480.6}$ lines, achieved within the period of the pulse, on the RF generator power at various τ and τ_{on}/τ. Curves 1–4 correspond to I_m of atomic lines with different duty cycles: continuous operation (1), 25% (2), 50% (3), 17% (4). Curves 5–8 correspond to I_m of ionic lines with different duty cycles: continuous operation (5), 25% (6), 50% (7), 17% (8).

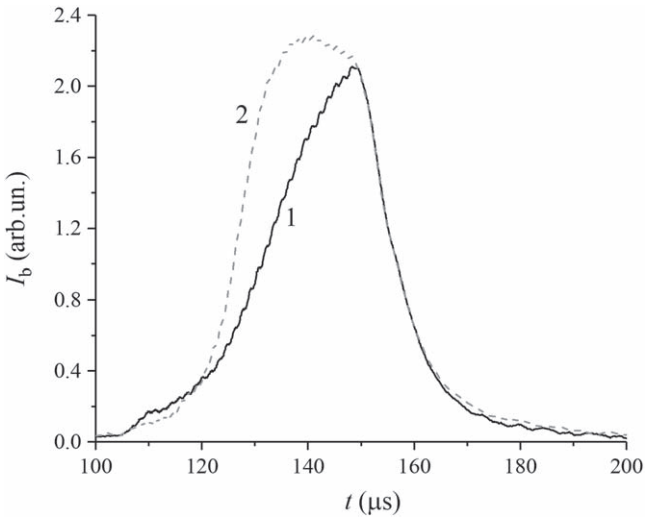

Figure 11. Time dependencies of the ion current I_b obtained in experiments with hybrid (1) and inductive (2) discharges.

metastable state. The Ar_2 resonant state is depopulated as a result of ionization by electrons, collisions of the second kind with electrons, radiative decay, and on the walls of the plasma source.

A detailed description of the numerical model is placed in the Appendix. Here we note that the power absorbed by the plasma W is determined by the current flowing through the antenna I_a and the equivalent plasma resistance R_{pl}, which depends on the electron concentration n_e and temperature T_e:

$$W = \frac{1}{2} I_a^2 R_{pl}(n_e, T_e, t). \quad (2)$$

The current I_a flowing through the antenna can be found by knowing the power of the RF generator P_{gen} and the resistance of the antenna, based on the equation:

$$P_{gen} = \frac{1}{2} I_a^2 (R_{ant} + R_{pl}(n_e, T_e, t)) \quad (3)$$

Equation (3) shows that in an inductive RF discharge, the RF generator power is divided between two loads: the active resistance of the external circuit and the equivalent plasma resistance, which determines the ability of the plasma to absorb RF power [23, 27]. Figure 15 show the dependence of the equivalent plasma resistance on the electron density, calculated by the formulas of [27–29]. A feature of the $R_{pl}(n_e)$ function is the fact that it depends nonmonotonically on electron density. In the region of small n_e, the equivalent resistance increases due to an increase in the number of electrons involved in the absorption of RF power, and at large n_e, R_{pl} falls due to a decrease in the width of the skin

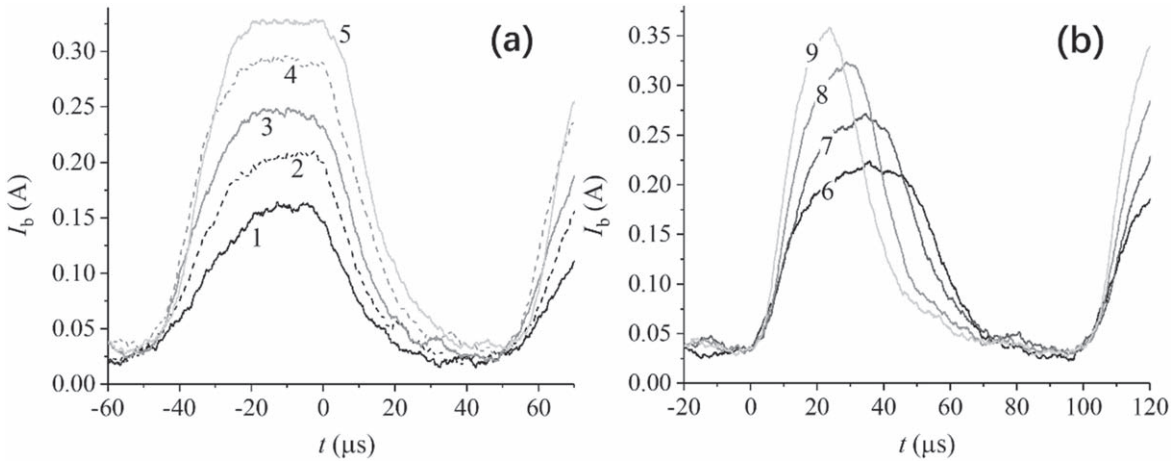

Figure 12. Time dependence of the extracted ion current I_b at various RF generator powers (a) and duty cycles (b). $\tau = 100$ μs. Curves 1–5 correspond to $\tau_{on} = 50$ μs and values of P_{gen}: 80 W (1), 100 W (2), 120 W (3), 160 W (4), 200 W (5). Curves 6–9 correspond to $P_{av} = 100$ W and values of τ_{on}: 50 μs (6), 40 μs (7), 30 μs (8), 22 μs (9).

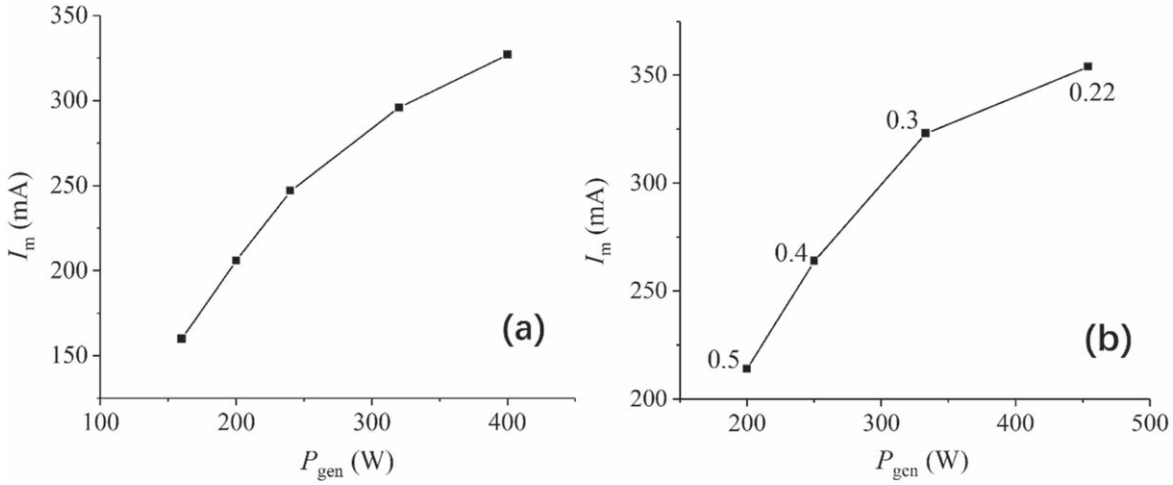

Figure 13. Dependence of the maximum (equilibrium) values of the ion current on the RF generator power (a) and the duty cycle (b). Dependence (b) is taken with fixed $P_{av} = 100$ W.

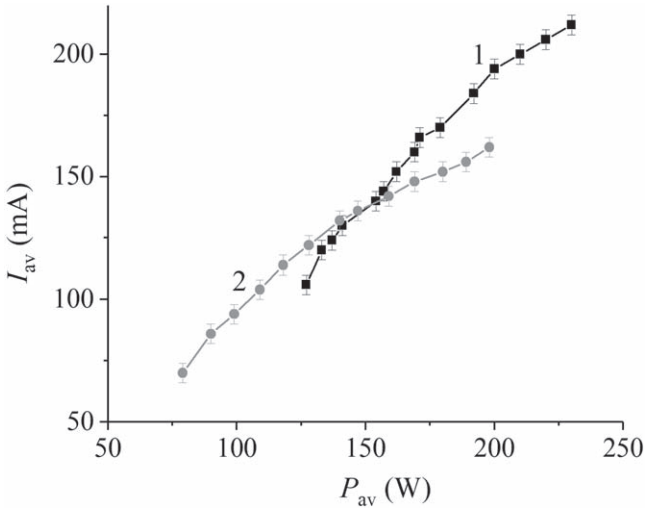

Figure 14. Dependence of the time-averaged ion current I_{av} on the average power of the RF generator P_{av}, obtained in stationary (1) and pulse-modulated (2) modes of the RF IIS operation. Pulsed mode frequency was 10 kHz with a duty cycle of 50%.

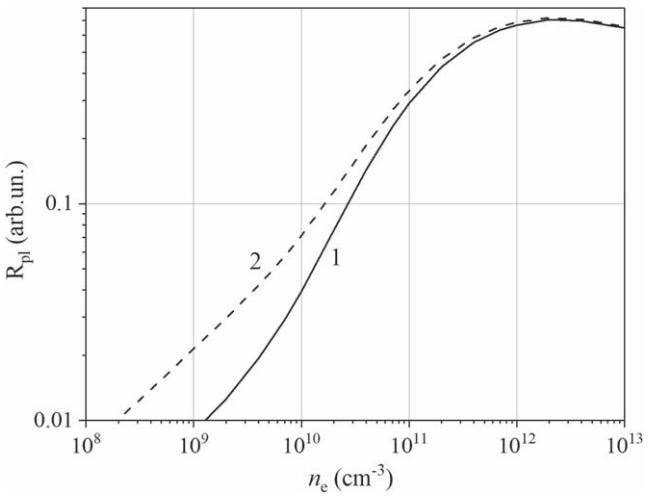

Figure 15. Dependence of the equivalent plasma resistance on the electron concentration, calculated for different argon pressures: 0.4 mTorr (1), 1 mTorr (2). An external magnetic field is absent.

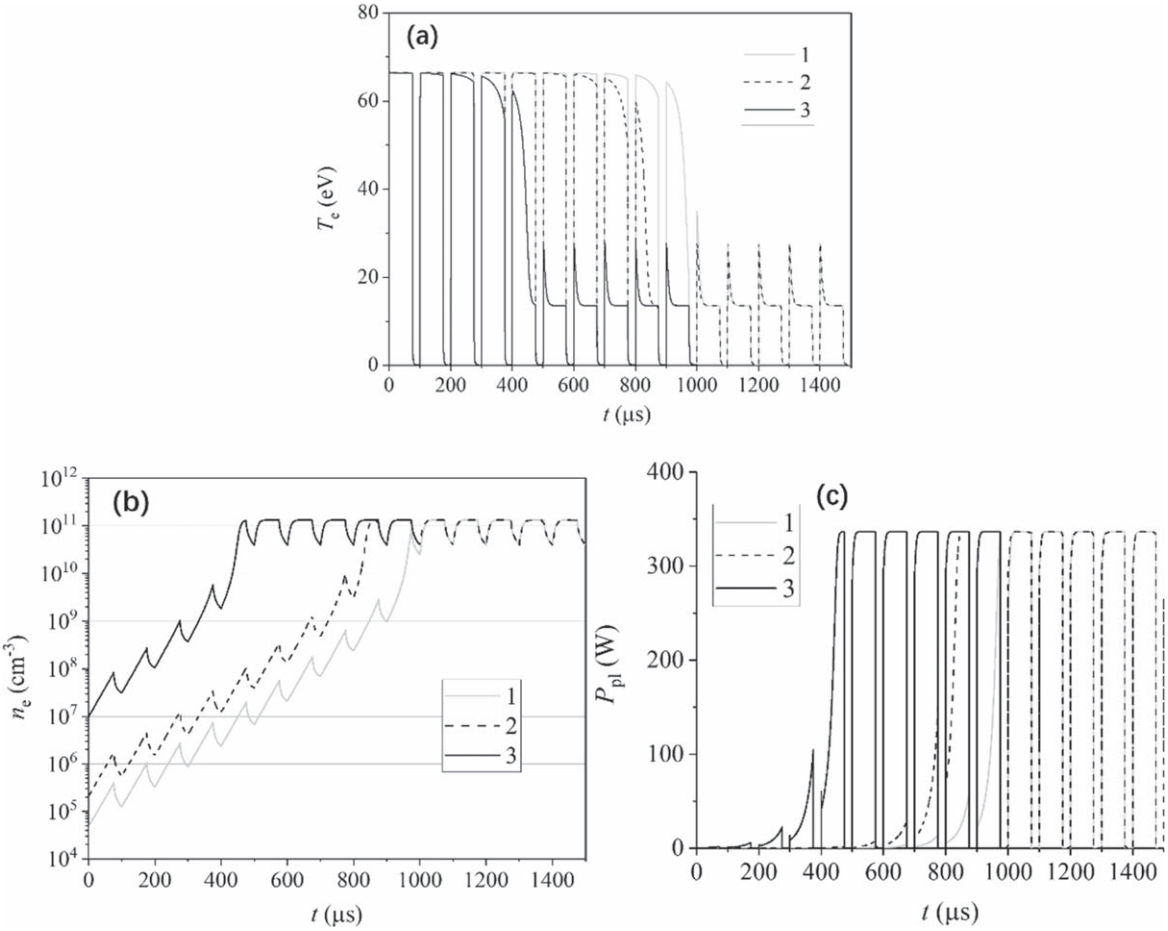

Figure 16. Time dependence of the electron temperature (a), concentration (b), and RF power coupled to plasma (c), calculated for different values of the initial plasma density: $n_{e0} = 10^7$ cm^{-3} (1), $n_{e0} = 10^5$ cm^{-3} (2), $n_{e0} = 10^4$ cm^{-3} (3).

layer where absorption occurs. In an inductive RF discharge without a magnetic field, as a rule, the plasma concentration does not exceed 3×10^{11} cm^{-3}. In this region, n_e, the values of R_{pl} and, consequently, P_{pl} increase with plasma concentration. When performing calculations, it was assumed that the RF voltage pulse had a rectangular shape. The RF voltage frequency was 13.56 MHz.

5. Results and discussion

5.1. Approaching a steady-state mode

A pulse-modulated inductive RF discharge is a sequence of RF voltage pulses of duration τ_{on} supplied to the plasma source antenna, separated by the time interval τ_{off}, when the amplitude of the applied voltage is equal to zero. The experimenter (unless special measures are taken) deals with a steady-state process resulting from thousands of RF voltage cycles. Let us consider how the steady-state mode of a pulse-modulated discharge is achieved immediately after the RF generator is turned on. By a steady process, the authors mean a process in which the change in plasma parameters becomes the same from pulse to pulse.

In the previous section, it was pointed out that the present model did not describe gas breakdown. Let us assume that, after breakdown, a quasi-neutral plasma appears in the discharge with an initial concentration n_{e0} and consider how the time required for the realisation of steady-state characteristics of the discharge depends on different n_{e0}. The calculated time dependencies of electron density and temperature, as well as the fraction of the power of the RF generator absorbed by the plasma P_{pl}, are shown in figure 16. It can be seen that the concentration and temperature of electrons in the steady-state discharge mode differ significantly from the values that exist in the discharge during the first single pulses. The reason for the difference can be easily understood by comparing the dependencies $n_e(t)$, $T_e(t)$, and $P_{pl}(t)$. For small values of n_e, which are realized after the ignition of the discharge, the values of the equivalent plasma resistance are small. As a consequence, the power absorbed by the plasma P_{pl} is low, and the electron temperature required for sustaining the discharge is high. If, during the first pulses, the power deposited in the discharge during the active part of the pulse leads to an increase in the electron density by Δn_{on}, which is greater than the decrease in the plasma density in the stage of its deionisation Δn_{off}, then the plasma density increases with time. With each subsequent pulse, n_e and P_{pl} self-consistently grow until a

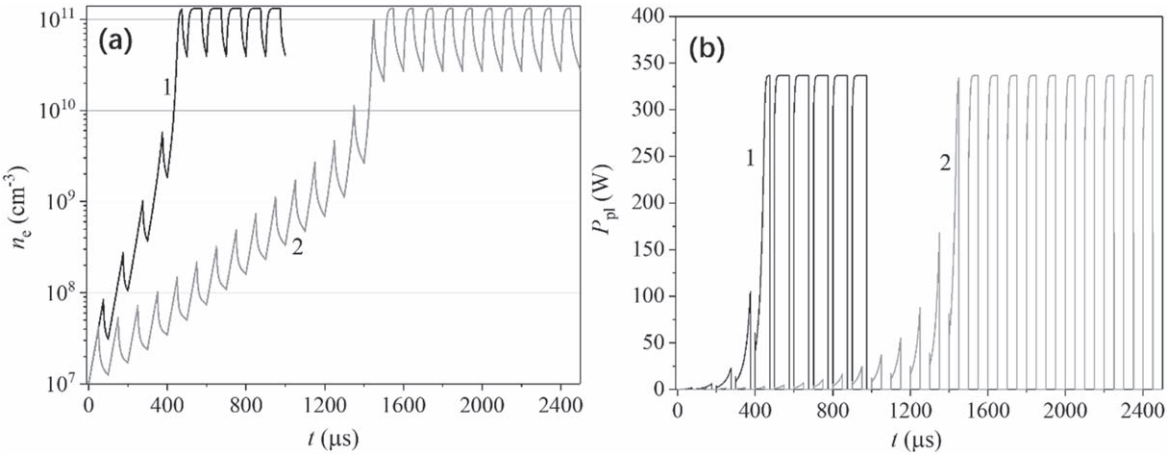

Figure 17. Time dependencies of the electron density (a) and the power coupled to the plasma (b) in the discharge, calculated at τ_{on}/τ values of 75% (1) and 50% (2). $\tau = 100$ μs. $P_{gen} = 400$ W, $R_{ant} = 1$ Ω.

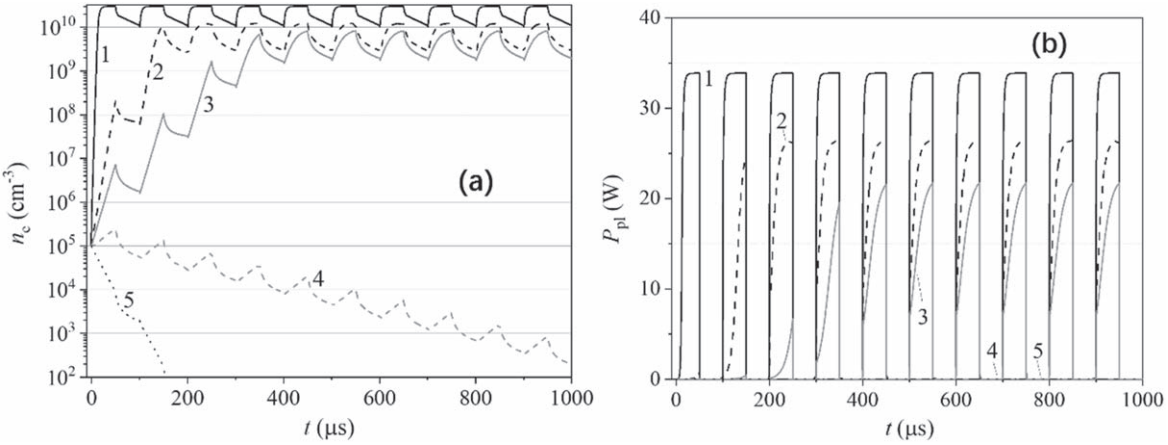

Figure 18. The time dependence of the electron concentration (a) and RF power coupled to plasma (b) for different pressures: 1 mTorr (1), 0.45 mTorr (2), 0.4 mTorr (3), 0.35 mTorr (4), 0.3 mTorr (5). $P_{gen} = 50$ W, $n_{e0} = 10^5$ cm^{-3}, $\tau = 100$ μs, $\tau_{on}/\tau = 0.5$, $R_{ant} = 1$ Ω.

steady-state discharge is established. Obviously, the higher the initial concentration, the faster the steady state is reached.

Similar considerations make it possible to explain the regularities in achieving a steady-state discharge mode when the ratio between the durations τ_{on}, τ_{off} changes (see figure 17). Indeed, the longer the active time of the pulse, the greater the increase in the electron concentration and the value of Δn_{on}. Accordingly, the shorter the deionisation time, the smaller the value of Δn_{off}. This leads to a significant acceleration in the approaching of a steady-state discharge mode.

Figure 18 shows the change in plasma parameters with time at various argon pressures, provided that $\tau = 100$ μs and $\tau_{on}/\tau = 0.5$. The initial plasma concentration was taken equal to $n_{e0} = 10^5$ cm^{-3}. Calculations showed that if the argon pressure was less than 0.4 mTorr, then during the deionization time, the electron density dropped below the initial value. This leads to a gradual decrease in the time-averaged plasma density and discharge extinction. With an increase in pressure, when the equivalent resistance of the plasma and the fraction of the absorbed power absorbed increase, the plasma concentration increases with each subsequent RF voltage pulse, and the discharge can be stable. The higher the pressure (the higher the equivalent plasma resistance), the faster the steady-state discharge mode is reached.

5.2. Parameters of a steady-state plasma

The patterns of achieving equilibrium (maximum) values of the plasma density within one pulse are close to the patterns of achieving a steady state. Figures 19 and 20 show the change in time of the main discharge characteristics, i.e. the electron density and temperature, the concentration of atoms in the metastable and resonant states, calculated at different powers of the RF generator. It is convenient to analyze the time dependencies of the main discharge parameters by presenting the results on a semi-logarithmic scale (see figure 21).

At the beginning of the active part of the pulse, a jump in the electron temperature is observed, which ensures a rapid increase in electron density and the number of excited atoms. In the steady state, the electron concentration does not fall

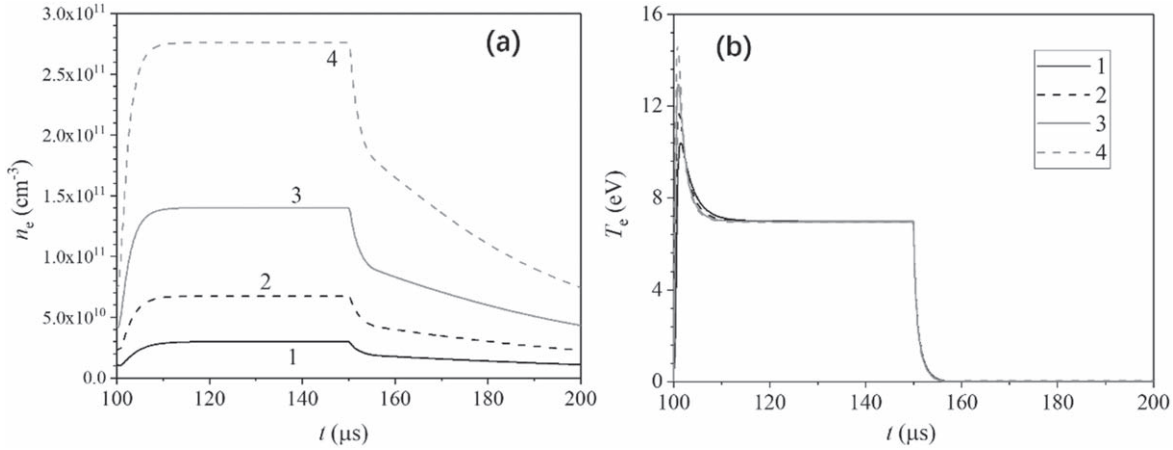

Figure 19. Dependence of the electron density (a) and temperature (b) on time, calculated at different powers of the RF generator: 50 W (1), 100 W (2), 200 W (3), 400 W (4). $\tau_{on}/\tau = 0.5$, $\tau = 100$ μs, pressure is 1 mTorr.

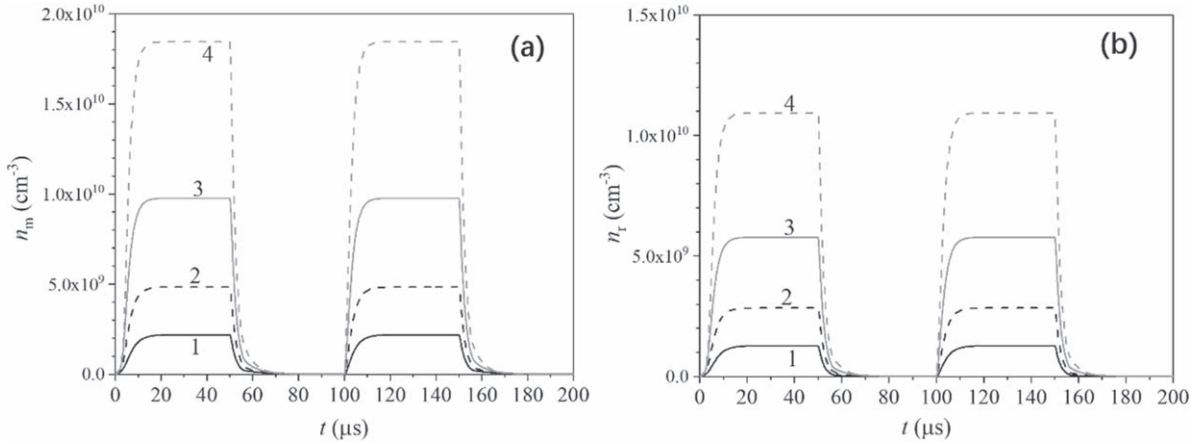

Figure 20. Dependence of the metastable (a) and resonant (b) atom concentrations on time, calculated at different powers of the RF generator: 50 W (1), 100 W (2), 200 W (3), 400 W (4). τ_{on}/τ =0.5, $\tau = 100$ μs, pressure is 1 mTorr.

below 10^9 cm^{-3} during τ_{off}, so the time to reach equilibrium values does not exceed 10 μs. After the equilibrium values are reached, the plasma characteristics do not change until the time τ_{on} has elapsed. After the end of the active part of the pulse, the electron temperature rapidly drops until it approaches some values that change slightly with time. The rate of decrease in the concentration of metastable and resonant atoms is much higher than the rate of decrease in electron density and is close to each other. This is due to the fact that at electron concentrations of the order of 10^{11} cm^{-3}, the populations of two closely spaced energy levels come into thermodynamic equilibrium [30]. Their lifetime is determined by the probability of radiative decay of the resonant level.

Electron density after the end of the active part of the pulse begins to fall rapidly, because as a result of a drop in the electron temperature, the number of fast electrons capable of ionising atoms decreases. Then the falling speed of n_e slows down. Here, the dominant processes that determine the rate of the plasma density fall are the escape of ions to the GDC walls and three-particle recombination. Its rate noticeably

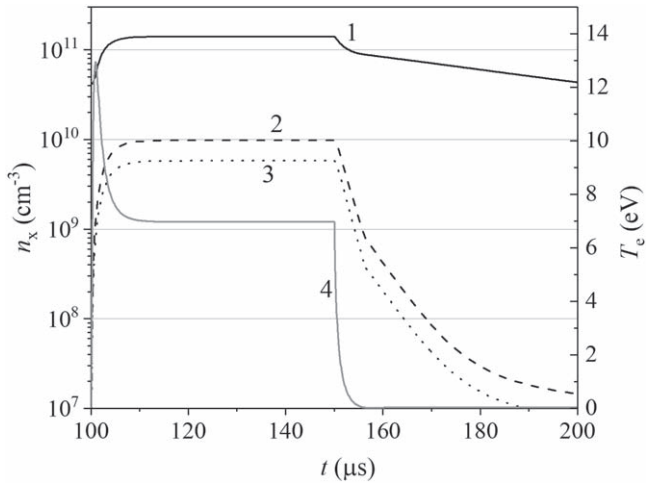

Figure 21. Time dependencies of the concentration of electrons (1), metastable atoms (2), resonant atoms (3) and electron temperature (4). $P_{gen} = 200$ W, $\tau_{on}/\tau = 0.5$, τ =100 μs, pressure is 1 mTorr.

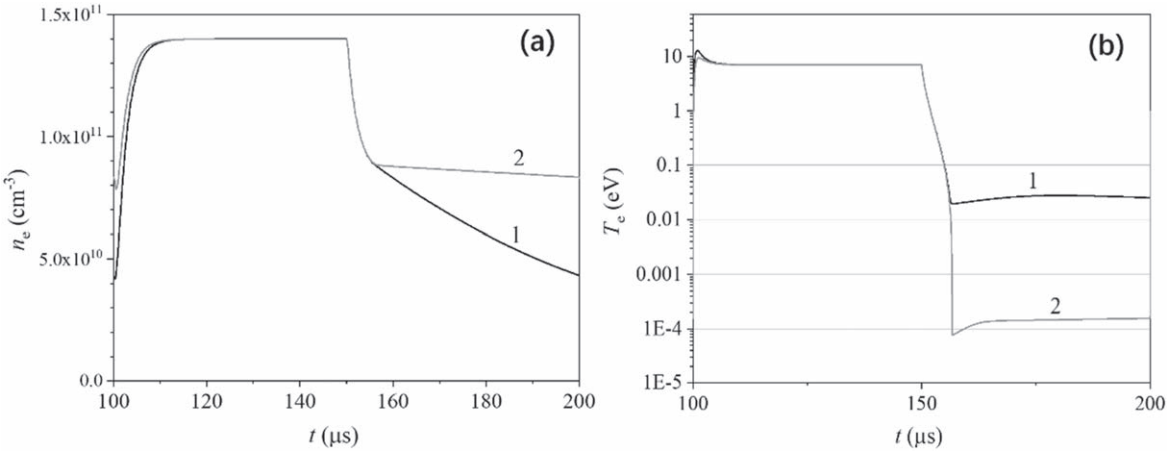

Figure 22. Dependence of the electron density (a) and temperature (b) on time, calculated with (1) and without (2) taking into account three-body recombination at an RF generator power of 200 W. $\tau_{on}/\tau = 0.5$, $\tau = 100$ μs, pressure is 1 mTorr.

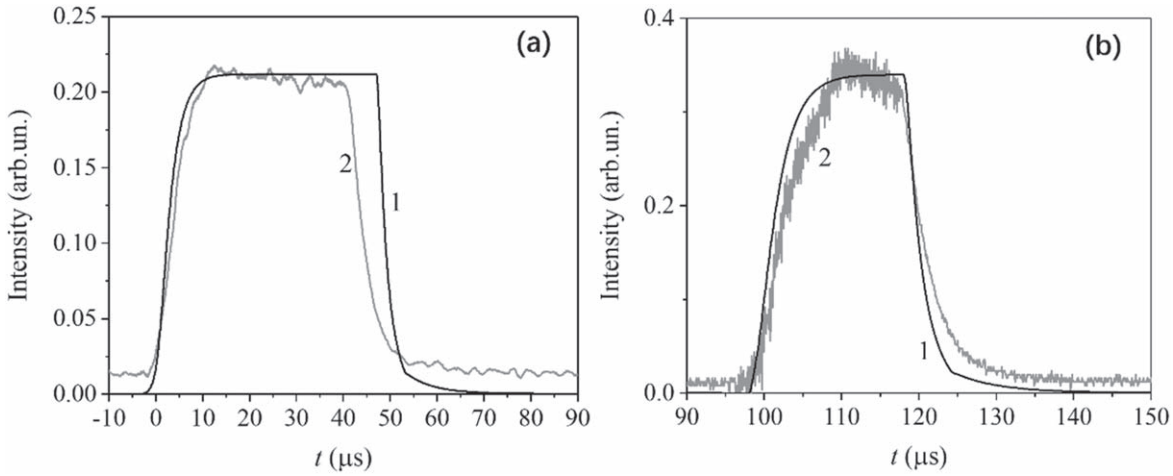

Figure 23. Comparison of the normalized experimental (2) and calculated (1) time dependencies of the atomic line radiation intensity.

increases as a result of a drop in the electron temperature. The contribution of volume recombination to the decrease in n_e can be traced by considering figure 22, which shows the results of plasma density calculations with and without recombination. As expected, the absence of the three-particle recombination leads to a much faster drop in the electron concentration in the deionisation stage. The electron temperature, on the contrary, increases, because as a result of recombination, energy is released, which leads to the heating of the electrons. The probability of Penning ionisation at the considered argon pressures is vanishingly small.

Figure 23 shows a comparison of the measured and calculated dependencies of the radiation intensity of argon atomic lines. Taking into account that in the calculations, it was assumed that the pulse shape had a strictly rectangular shape, and in the experiment, the time of the leading and trailing edges of the pulse was 5–10 μs, the agreement between the measured and calculated curves can be considered satisfactory. In addition, it should be noted that, just as in the experiment, the calculated equilibrium values of the plasma density are proportional to the power of the RF generator.

Now let us try to explain why the growth of P_{gen} is accompanied by a slowdown in the growth of the ion beam current I_b. To do this, the calculated dependencies of the RF generator power required to extract the ion current of a given value from the argon consumption are considered (see figure 24). The calculations were performed based on a stationary model of an inductive RF discharge [23]. One can see that, as the argon consumption decreases, the $P_{gen}(f_v)$ curves grow sharply. In this region, the increase in power P_{gen} is accompanied by a lower increase in the ion current than in the region of large f_v (see figure 25). Thus, in the region of low flow rates, significantly higher energy input to the discharge is required to increase the values of I_b. This leads to a slowdown in the growth of the $I_b(P_{gen})$ and $I_b(\tau_{on}/\tau)$ curves and a decrease in the efficiency of the pulse-modulated discharge mode compared to the continuous one. The reason is that in the active part of the pulse, the power of the RF generator is several times higher than the average power. Here, sooner or

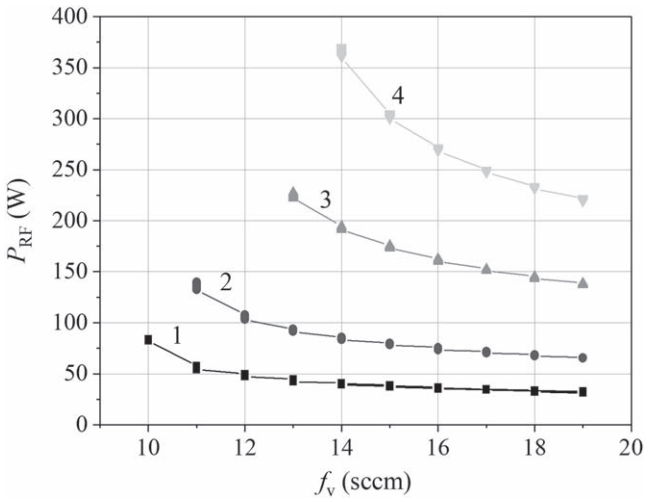

Figure 24. Dependence of the RF generator power required to extract the ion current of a given value I_{ion} on the argon consumption. Curves correspond to different values of I_{ion}: 50 mA (1), 100 mA (2), 200 mA (3), 300 mA (4).

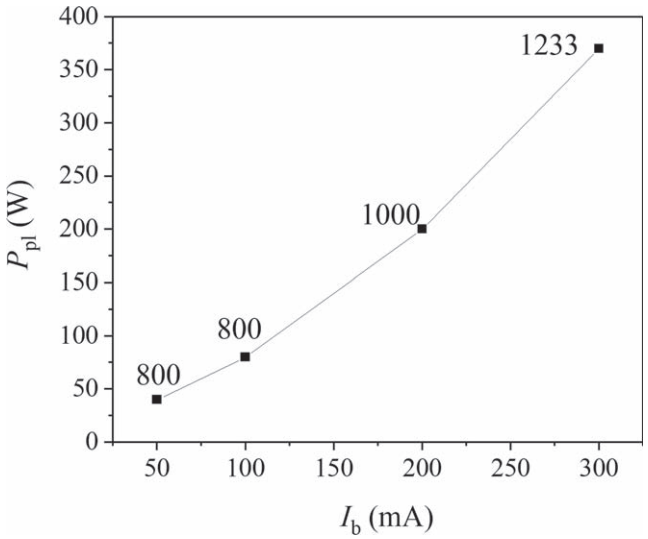

Figure 25. Dependence of the RF power, necessary for the extraction of the ion beam I_b at argon flow rate of 14 sccm. Numbers above the curve show corresponding ion cost (W/A).

later, the discharge passes into a mode in which the rate of the ion current growth begins to saturate with increasing RF power.

Figure 26 shows calculated ion beam currents I_b. Comparison with experimentally measured values presented in figure 12 shows general agreement with a few differences. Since the resistance of the RF antenna and the neutral gas pressure were not measured in the experiments, arbitrary values were taken for the numerical simulation, resulting in different absolute values of I_b. The dependence of maximum (equilibrium) values of I_b is more linear in the numerical simulation, because the decrease in the density of neutral gas due to ions leaving the GDC as I_b was not considered in the calculations. Apart from that, one can see that I_b rise time on

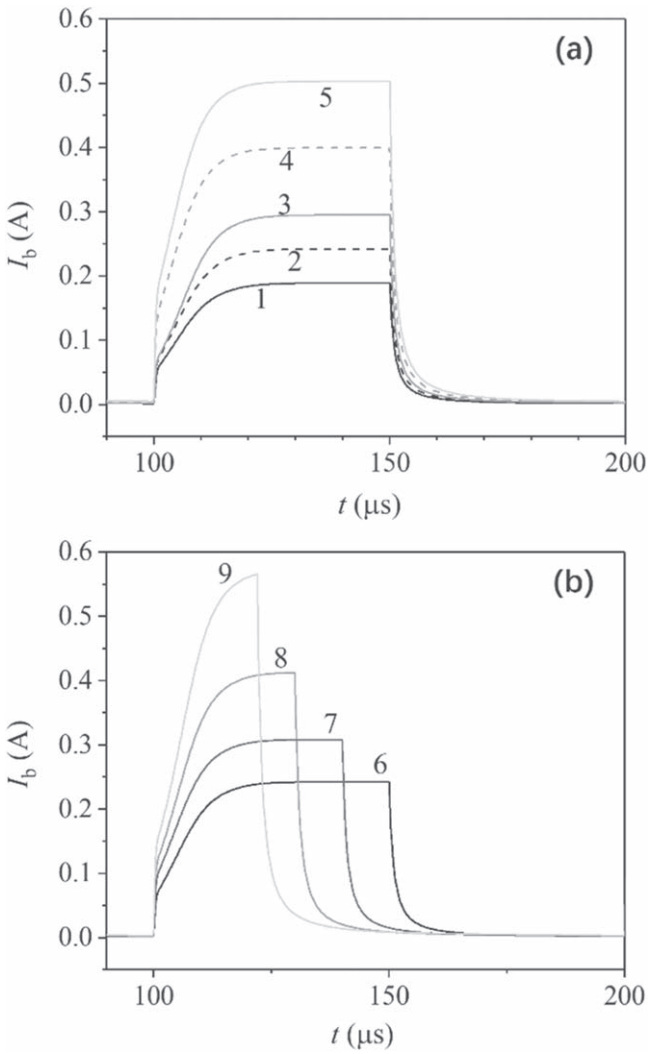

Figure 26. Time dependence of the extracted ion current I_b calculated at various RF generator powers (a) and duty cycles (b). $\tau = 100$ μs, $R_{ant} = 1$ Ω, $p = 0.45$ mTorr, IOS transparency for atoms and ions is 0.6. Curves 1–5 correspond to $\tau_{on} = 50$ μs and values of P_{gen}: 80 W (1), 100 W (2), 120 W (3), 160 W (4), 200 W (5). Curves 6–9 correspond to $P_{av} = 100$ W and values of τ_{on}: 50 μs (6), 40 μs (7), 30 μs (8), 22 μs (9).

the leading edge and fall time after the end of the active part of the pulse are smaller than those in the experiment. The former is caused by the noninstantaneous rise of the RF current through the antenna, which can be seen in figure 3. In the numerical simulation the rectangular shape of the pulse was assumed, while in the experiment rise time of the RF antenna current usually is about 10 μs and is strongly influenced by the matching circuit and the RF generator. Shorter I_b fall time needs additional investigation.

6. Conclusions

In the present work, an experimental study of the characteristics of a pulse-modulated RF discharge at pressures typical for the operating modes of RF gridded ion sources, was carried out. The values of the ion current extracted

from an RF inductive source operating in stationary and pulse-modulated modes were compared. In addition, the experimental data were compared with the results of numerical calculations based on a 0D global model of the discharge.

The experiments have shown that, at an RF generator power of 100 W, the intensity of atomic lines and the ion current reach stationary values in a time of about 20 μs. For larger values of P_{gen}, this value is reduced to 10 μs. The decrease in the intensity of plasma radiation and the ion current after turning off the RF generator occurs over times of the order of 15 μs. These times are significantly lower than those observed in [5] at higher argon pressures. The present experiments confirmed that the main reason for the delay in the establishment of equilibrium, as suggested by the authors of [5], was the capacitive component of the discharge. The calculations performed under the assumption that the discharge is in the inductive mode during the entire pulse duration turned out to be close to the experimental data presented in section 3.

Experimental and calculated data indicate that direct excitation and ionization are the dominant processes that determine the equilibrium electron concentration in the steady-state discharge. The contribution of stepwise processes is not large, which reduces the possibility of increasing the energy efficiency of RF ion sources when replacing the continuous mode with a pulse-modulated one.

Calculations have shown that the plasma density increases with time if the power deposited in the discharge during the first pulses after the ignition is greater than a certain value. This value is determined by the equality between the increase in the electron concentration Δn_{on} during the active part of the pulse and the decrease Δn_{off} in the stage of deionization. With each subsequent pulse, n_{e} and P_{pl} self-consistently grow until a steady-state discharge occurs. Obviously, the higher the initial concentration, the faster the steady state is realised. If Δn_{on} is less than Δn_{off}, then the discharge in the plasma source cannot exist.

The calculations showed a strong dependence of the process of achieving the steady-state operation of the ion source on the equivalent plasma resistance, i.e. on the ability of the plasma to absorb RF power.

The measurements showed that the pulse mode of operation of the RF inductive ion source had a noticeable advantage at low powers of the RF generator. However, as P_{gen} increases, the advantage is lost, because in the active part of the pulse, the power of the RF generator is several times higher than the average power. Here, sooner or later, the discharge passes into a mode in which the rate of growth of the ion current with increasing power begins to saturate.

Acknowledgments

This work was supported by the Russian Science Foundation (No. 21-72-10090), https://rscf.ru/en/project/21-72-10090/.

Appendix

The equation describing the change in time of the concentration of ions in the discharge has the form:

$$V\frac{\partial n_{\text{i}}}{\partial t} = n_{\text{e}}\sum_{l=0}^{2} n_l \langle \sigma_{l\text{i}} v\rangle V + n_1^2 k_{\text{p}} V - n_{\text{e}}^2 n_{\text{i}} k_{\text{rec}} V - n_{\text{i}} v_{\text{i}} S, \tag{A1}$$

where n_l is the concentration of atoms in the lth energy state; the values of the parameter l are equal to 0, 1 and 2 corresponding to atoms in the ground, metastable, and resonant states; n_{i}, n_{e} are the concentrations of ions and electrons; $\sigma_{l\text{i}}$ is the ionization cross section of atoms in the state l, the sign $\langle\rangle$ means averaging this cross section over the electron distribution function; k_{p}, k_{rec} are the rates of Penning ionisation and three-particle electron–ion recombination; V is the volume of the plasma source, S is the surface of the plasma source; v_{i} is the ion velocity determined by the Bohm formula:

$$v_{\text{i}} = 0.4\sqrt{\frac{2kT_{\text{e}}}{M}}, \tag{A2}$$

where T_{e} is the electron temperature, k is the Boltzmann constant, and M is the ion mass.

The change in the number of electrons with time is described by an equation similar to equation (A1):

$$V\frac{\partial n_{\text{e}}}{\partial t} = n_{\text{e}}\sum_{l=0}^{2} n_l \langle \sigma_{l\text{i}} v\rangle V + n_1^2 k_{\text{p}} V - n_{\text{e}}^2 n_{\text{i}} k_{\text{rec}} V - n_{\text{i}} v_{\text{e}} S. \tag{A3}$$

Equation (A3) differs from equation (A1) by the last term of the equation, which describes the rate of electron escape to the walls. The thermal escape velocity of electrons v_{e} is determined by the formula:

$$v_{\text{e}} = \frac{1}{4}\sqrt{\frac{8kT_{\text{e}}}{\pi m}}\exp\left(-\frac{eV_{\text{pl}}}{T_{\text{e}}}\right), \tag{A4}$$

where m is the mass of electrons, V_{pl} is the plasma potential relative to the GDC walls.

The change in the number of metastable atoms with time is described by the equation:

$$V\frac{\partial n_1}{\partial t} = n_{\text{e}}\sum_{l\neq 1} n_l \langle \sigma_{l1} v_{\text{e}}\rangle V + n_{\text{e}}^2 n_{\text{i}} k_{\text{rec}}^{\text{m}} V - n_{\text{e}} n_1 \langle \sigma_{1\text{i}} v_{\text{e}}\rangle V - n_{\text{e}}\sum_{l\neq 1} n_1 \langle \sigma_{1l} v_{\text{e}}\rangle V - n_{\text{m}}^2 k_{\text{p}} V - n_1 v_0 S, \tag{A5}$$

where σ_{lj} is the cross section for the transition of an atom from the lth energy state to the state j in a collision with electrons, v_0 is the thermal velocity of atoms determined by the gas temperature T_{g}:

$$v_0 = \frac{1}{4}\sqrt{\frac{8kT_{\text{g}}}{\pi M}} \tag{A6}$$

The equation for the concentration of atoms in the resonant state differs from equation (A5) by the term describing the radiative decay of the level.

$$V = \frac{\partial n_2}{\partial t} = n_e \sum_{l \neq 2} n_l \langle \sigma_{l2} v_e \rangle V + n_e^2 n_i k_{rec}^2 V - n_e n_2 \langle \sigma_{2i} v_e \rangle V - n_e \sum_{l \neq 2} n_1 \langle \sigma_{2l} v_e \rangle V - n_2 A_{20}^* - n_e v_2 S \quad \text{(A7)}$$

where A_{20} is the effective probability of the transition of an atom from the resonant to the ground state. In the presence of radiation trapping, the values A_{20}^* are related to the probability of radiative decay of the resonance level by the equation [30]:

$$A_{20}^* = A_{20} \frac{1}{\kappa_0 r \sqrt{\ln(\kappa_0 r)}}, \quad \text{(A8)}$$

where κ_0 is the absorption coefficient at the line centre and r is the radius of the plasma source. The absorption coefficient is determined by the expression [30]:

$$\kappa_0 = \frac{\lambda_{lj}^4}{8\pi} \frac{g_j}{g_l} n_j A_{lj} 2 \frac{\sqrt{\ln 2}}{c \Delta\lambda_D \sqrt{\pi}}, \quad \text{(A9)}$$

where λ_{lj} is the wavelength of the transition from level l to level j; g_l, g_j are the statistical weights of levels l and j; $\Delta\lambda_D$ is the width of the Doppler contour.

The quasi-neutrality equation has the form:

$$n_e = n_i. \quad \text{(A10)}$$

The change in electron temperature with time is described by the equation:

$$\frac{3}{2} n_e \frac{\partial T_e}{\partial t} V = W - 2T_e n_e v_e S - V_{pl} n_i v_i S - \sum_{l=0}^{2} U_{li} n_l n_e \langle \sigma_{li} v_e \rangle V - \sum_{l=0}^{1} \sum_{j>1} U_{lj} n_l n_e \langle \sigma_{lj} v_e \rangle V - \sum_{l=1}^{2} \sum_{j<1} U_{lj} n_l n_e \langle \sigma_{lj} v_e \rangle V - n_2 A_{20}^* U_{02} + U_{01} n_1^2 k_p V + n_e^2 n_i V \sum_{l=1}^{2} U_{li} k_{rec}^l, \quad \text{(A11)}$$

where U_{0i}, U_{1i}, U_{2i}, U_{01}, U_{02} are the ionisation energy of atoms in the ground, metastable, and resonant states, the excitation energy of the metastable and resonant levels; $U_p = 2U_{01} - U_{0i}$.

The concentration of atoms in the ground state is determined by the pressure p:

$$n_0 = \frac{p}{kT_g}. \quad \text{(A12)}$$

Equations (A1) and (A3) differ only in the last terms on the right hand side of the equations. Taking into account the quasi-neutrality equation (A10) and equating the right hand sides of equations (A1) and (A3), one can obtain an expression for the plasma potential with respect to the walls:

$$V_{pl} = -T_e \ln\left(0.8 \sqrt{\frac{\pi m}{M}}\right) \quad \text{(A13)}$$

When performing calculations, the cross sections for excitation and ionisation of the argon energy levels were calculated using the formulas of Gryzinsky [31].

The deexcitation cross sections for the argon energy levels by electrons were calculated from the known excitation cross sections based on the Klein–Rosseland formula, which follows from the principle of detailed balance [30]:

$$\sigma_{lj}(\varepsilon) = \frac{g_j}{g_l} \frac{\varepsilon + U_{0j} - U_{0l}}{\varepsilon} \sigma_{jl}(\varepsilon + U_{0j} - U_{0l}), \quad \text{(A14)}$$

where ε is the electron energy.

The value of the Penning ionisation rate used was equal to $k_p = 6.3 \times 10^{-10}$ cm^3, and the three-particle recombination rate was equal to $k_{rec} = 10^{-19} (T_e \times 11600/300)^{-4.5}$ cm^6 s^{-1} [3] where T_e was taken in eV.

References

[1] Lisovskiy V A *et al* 2017 *Vacuum* **145** 194
[2] Musil J *et al* 2001 *J. Vac. Sci. Technol.* A **19** 420
[3] Bogaerts A and Gijbels R 1995 *Phys. Rev.* A **52** 3743
[4] Hebner G A and Fleddermann C B 1997 *J. Appl. Phys.* **82** 2814
[5] Han J *et al* 2020 *Phys. Plasmas* **27** 063509
[6] Park J H *et al* 2017 *Plasma Sources Sci. Technol.* **26** 055016
[7] Saikia P *et al* 2017 *Phys. Plasmas* **24** 013503
[8] Tang X M and Manos D M 1999 *Plasma Sources Sci. Technol.* **8** 594
[9] Lieberman M A and Ashida S 1996 *Plasma Sources Sci. Technol.* **5** 145
[10] Subramonium P and Kushner M J 2004 *Appl. Phys. Lett.* **85** 721
[11] Ramamurthi B and Economou D J 2002 *Plasma Sources Sci. Technol.* **11** 324
[12] Subramonium P and Kushner M J 2002 *J. Vac. Sci. Technol.* A **20** 325
[13] Lymberopoulos D P, Kolobov V I and Economou D J 1998 *J. Vac. Sci. Technol.* A **16** 564
[14] Gao F *et al* 2019 *J. Appl. Phys.* **126** 093302
[15] Lv X Y *et al* 2021 *Chin. Phys.* B **30** 045202
[16] Han J *et al* 2019 *Phys. Plasmas* **26** 103503
[17] Qu C H, Nam S K and Kushner M J 2020 *Plasma Sources Sci. Technol.* **29** 085006
[18] Goebel D M and Katz I 2008 *Fundamentals of Electric Propulsion: Ion and Hall Thrusters* (Hoboken: Wiley)
[19] Mazouffre S 2016 *Plasma Sources Sci. Technol.* **25** 033002
[20] Groh K H and Loeb H W 1991 *J. Prop. Power* **7** 573
[21] Killinger R, Leiter H and Kukies R 2007 RITA ion propulsion systems for commercial and scientific applications *Proc. of the 43rd AIAA/ASME/SAE/ASEE Joint Propulsion Conf. & Exhibit (Cincinnati)* (AIAA)
[22] Kralkina E A *et al* 2019 *Vacuum* **167** 136
[23] Kralkina E A *et al* 2017 *Plasma Sources Sci. Technol.* **26** 055006
[24] Kralkina E *et al* 2020 *Plasma Sci. Technol.* **22** 055405
[25] Masherov P E, Riaby V A and Godyak V A 2016 *Rev. Sci. Instrum.* **87** 02B926
[26] Kral'kina E A 2008 *Phy.-Usp.* **51** 493
[27] Kralkina E A *et al* 2016 *Plasma Sources Sci. Technol.* **25** 015016
[28] Vavilin K V *et al* 2004 *Tech. Phys.* **49** 565
[29] Kralkina E A *et al* 2018 *AIP Adv.* **8** 035217
[30] Biberman L M, Vorob'ev V S and Yakubov I T 1987 *Kinetics of Nonequilibrium Low-Temperature Plasma* (New York: Consultants Bureau)
[31] Gryziński M 1965 *Phys. Rev. J. Arch.* **138** A336